8th International Congress of Croatian Society of Mechanics
29 September – 2 October 2015
Opatija, Croatia

Damage modeling using higher-order finite element formulation

Filip PUTAR, Tomislav LESIČAR, Jurica SORIĆ, Zdenko TONKOVIĆ

Faculty of Mechanical Engineering and Naval Architecture
E-mails: filip.putar@fsb.hr, tomislav.lesicar@fsb.hr, jurica.soric@fsb.hr
zdenko.tonkovic@fsb.hr

Abstract

In the presented research, the two dimensional C^1 continuity triangular finite element is used for the modeling of the quasi-brittle softening phenomena. The implemented damage model is based on an isotropic damage law applied upon the higher-order stress-strain constitutive relations originating from the full strain gradient theory. Both homogeneous and heterogeneous materials are analyzed, where the material stiffness behavior is introduced in the computational model through the constitutive tensors obtained using the second-order homogenization procedure. Parametric analysis of the model is performed by changing the values of an internal length scale parameter. All the algorithms derived are implemented into the FE software ABAQUS via user subroutines. The verification of the presented computational model is performed on the benchmark example.

1 Introduction

Many engineering materials, such as polymers, concrete and composites after certain stress level start to show gradual decrease in the stiffness which is a direct consequence of the debonding of the atoms on the lower scales [1]. Since the straightforward modeling of these phenomena is still inappropriate from a computational point of view, numerical implementation of this so called softening behavior is mostly realized throughout some interventions in the constitutive model. For example, the isotropic damage introduces a damage variable in the constitutive model which carries the information about the material state at the lower scales. Softening behavior is always accompanied by high deformation gradients, i.e. strain tends to localize in the area where softening is occurring. With application of the classical continuum mechanics this strain localization cannot be properly resolved because material tangent stiffness modulus loses its positive definiteness at the onset of the softening [2]. Partial differential equations associated with a material damage then become ill-posed resulting in their loss of elliptic character. In the finite element environment this phenomenon can be noticed by gradual refinement of the mesh in the softening area, leading to physically unrealistic, mesh-dependent solutions instead of a converged state as it is expected. Strain tends to localize in the smallest possible volume, i.e. in the smallest finite element in this case, and the associated energy dissipation has a tendency to become zero [3].

Various regularization techniques have been developed in the past few decades to overcome this problem, but probably the most successful ones are those related to the non-locality. In the case of the non-local models stress at a point does not depend anymore only on the strain and other state variables at this point, but also on the strains and other state variables of the points surrounding this particular point of interest. Magnitude of this interaction is described by the internal length scale parameter which limits the localization of damage to the scale of the microstructure [2]. Basically, there are two different approaches when it comes to describing of non-locality in the model, integral and gradient approach. The integral approach, introduced in [3], is based upon spatial averaging of the state variables, typically strains, in the finite neighborhood of a certain point, leading to the very complicated constitutive relations made of convolution-type integrals. The gradient approach enhances the constitutive relation either by incorporation of the strain-gradients or by introduction of both strain-gradients and their stress conjugates. In the case when only strain-gradients are used as an enhancement of the constitutive relation, explicit and implicit gradient formulations are usually used when dealing with softening, either in elasticity context [4], plasticity context [5] or in the analysis of the elastic wave propagation [6, 7]. Second type of the gradient approaches where both strain-gradients and their stress conjugates enter the constitutive relation has been employed less often, mainly because it is numerically more complex. In the recent developments higher-order stress-strain theory has been employed in the context of a damage modeling of an infinitely long bar, where the authors concluded that the addition of the higher-order stress terms results in stabilizing the positive definiteness of tangent stiffness moduli when entering the strain softening regime. In such a way physically consistent solutions can be ensured and strain-softening phenomenon can be realistically reproduced [8]. Further development from one-dimensional to multi-dimensional simulation of a localized failure process has been made in [9]. Both in [8] and [9] EFG meshless method has been used for finding the approximate solutions to the corresponding boundary value problems. Another advantage of the higher-order stress-strain theory is that it can easily introduce material heterogeneity in the constitutive relations through the higher order material stiffness tangents linking the first-order stress to the second order strain and the second-order stress to the first-order strain [10]. Tangential material stiffness matrices can be obtained by applying the homogenization technique on the representative volume element (RVE) [11].

The present paper is organized as follows. Chapter 2 briefly discusses formulation and numerical implementation of the higher-order stress-strain damage theory in the C^1 continuity triangular finite element developed in [11]. In the Chapter 3 presented damage algorithm has been verified on the benchmark example from the literature, where both homogeneous and heterogeneous materials have been considered. The last chapter is reserved for some concluding remarks.

2 Higher-order finite element formulation for softening material

In this chapter an enhancement of a three-node C^1 continuity triangular finite element presented in [11] for application in the softening regime is given. Developed finite element is based on a second gradient continuum theory for which more details can be found in [12]. Relations describing the softening phenomena are presented, and afterwards finite element derivation with the softening behavior is shown.

2.1 Softening model

The classical constitutive relation of elasticity based damage mechanics reads [1]

$$\boldsymbol{\sigma} = (1 - D)\mathbf{C}\boldsymbol{\varepsilon}, \tag{1}$$

where D is the scalar damage variable describing local isotropic damage state. D can vary from 0 to 1, where 0 means that the material is still undamaged, while 1 denotes complete loss of material integrity. $\boldsymbol{\sigma}$, $\boldsymbol{\varepsilon}$ and $\mathbf{C}$ are tensors referring to Cauchy stress, strain and elastic stiffness, respectively. For the calculations conducted in this paper damage evolution is defined as

$$D = \begin{cases} \dfrac{k_u\left(\varepsilon_{eqv} - k_0\right)}{\varepsilon_{eqv}\left(k_u - k_0\right)} & k_0 \le \varepsilon_{eqv} \le k_u \\ 1 & \varepsilon_{eqv} > k_u \end{cases}, \tag{2}$$

where k_0 and k_u are the material constants representing the threshold strain at which damage is initiated and the strain at which material completely loses its stiffness, respectively. ε_{eqv} is the equivalent elastic strain measure which, considering the damage only due to the tensile strains, can be expressed as

$$\varepsilon_{eqv} = \sqrt{\left(\varepsilon_1\right)^2 + \left(\varepsilon_2\right)^2}, \tag{3}$$

with ε_1 and ε_2 denoting principal strain components of the strain tensor $\boldsymbol{\varepsilon}$. In the algorithms presented in this paper ε_{eqv} has the role of a history parameter, meaning that damage in a point will rise only if ε_{eqv} exceeds the highest value of the equivalent elastic strain already reached in this point. In the uniaxial stress situation Eq. (2) results in the linear softening and complete loss of the material coherence at $\varepsilon_{eqv} = \varepsilon = k_u$. Linear damage evolution law is often defined for the theoretical developments. Softening in the real materials is usually nonlinear and can be modelled with various evolution laws, e.g. exponential softening law or modified power law [2].

2.2 Derivation of the higher-order finite element with softening behavior

The element shown in Fig. 1 consists of three nodes, each having twelve degrees of freedom. The nodal degrees of freedom are the two displacements and their first- and second-order derivatives with respect to the Cartesian coordinates. The element describes plane strain state and its displacement field is approximated by the complete fifth order polynomial with 21 coefficients.

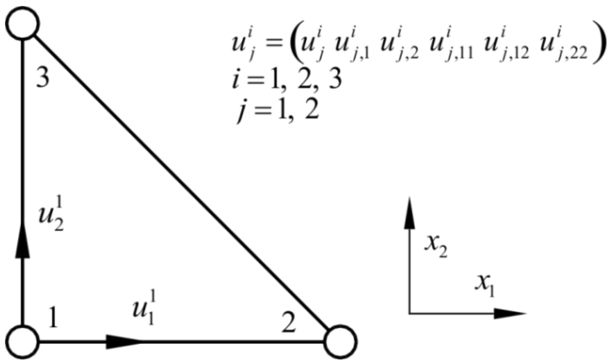

Figure1: C^1 triangular finite element [11]

The element equations are derived from the variation of the principle of virtual work, which for the strain gradient continuum reads

$$\int_A \delta\boldsymbol{\varepsilon}^T \boldsymbol{\sigma}\, \mathrm{d}A + \int_A \delta\boldsymbol{\eta}^T \boldsymbol{\mu}\, \mathrm{d}A = \int_s \delta\mathbf{u}^T \mathbf{t}\, \mathrm{d}s + \int_s \delta\left(\mathrm{grad}\,\mathbf{u}^T\right)\mathbf{T}\, \mathrm{d}s\,. \tag{4}$$

In Eq. (4) $\boldsymbol{\eta}$ is the second-order strain tensor compound of second derivatives of the displacement vector $\mathbf{u}$, while $\boldsymbol{\mu}$ is the work conjugate of the second-order strain, so-called double stress tensor. $\mathbf{t}$ and $\mathbf{T}$ are the traction tensor and the double traction tensor, respectively. Material softening is a highly non-linear process and therefore Eq. (4) has to be written in the incremental form where each increment starts from the last converged equilibrium state at the interval beginning t^{i-1}, and converges iteratively to a new affine equilibrium state at the interval ending t^i. The stress and the double stress increments, $\Delta\boldsymbol{\sigma}$ and $\Delta\boldsymbol{\mu}$, are computed by the incremental constitutive relations which, for the undamaged material, read

$$\begin{aligned} \Delta\boldsymbol{\sigma} &= \mathbf{C}_{\sigma\varepsilon}\Delta\boldsymbol{\varepsilon} + \mathbf{C}_{\sigma\eta}\Delta\boldsymbol{\eta}, \\ \Delta\boldsymbol{\mu} &= \mathbf{C}_{\mu\varepsilon}\Delta\boldsymbol{\varepsilon} + \mathbf{C}_{\mu\eta}\Delta\boldsymbol{\eta}. \end{aligned} \tag{5}$$

Herein $\mathbf{C}_{\sigma\varepsilon}$, $\mathbf{C}_{\sigma\eta}$, $\mathbf{C}_{\mu\varepsilon}$ and $\mathbf{C}_{\mu\eta}$ are the material tangent stiffness matrices which can be computed from the appropriate RVE using second-order homogenization procedure. If the material homogeneity, material isotropy and symmetry of the RVE are considered for the model problem, the material tangent stiffness matrices $\mathbf{C}_{\sigma\eta}$ and $\mathbf{C}_{\mu\varepsilon}$ are both zero [10]. In the context of the softening behavior it is assumed that all tangent stiffness matrices appearing in Eq. (5) are pre-multiplied with the term $(1-D)$. In that way, the non-linear constitutive damage model after linearization gives the following set of incremental constitutive relations

$$\begin{aligned} \Delta\boldsymbol{\sigma} &= (1-D^{i-1})\left(\mathbf{C}_{\sigma\varepsilon}\Delta\boldsymbol{\varepsilon} + \mathbf{C}_{\sigma\eta}\Delta\boldsymbol{\eta}\right) - \Delta D\left(\mathbf{C}_{\sigma\varepsilon}\boldsymbol{\varepsilon}^{i-1} + \mathbf{C}_{\sigma\eta}\boldsymbol{\eta}^{i-1}\right), \\ \Delta\boldsymbol{\mu} &= (1-D^{i-1})\left(\mathbf{C}_{\mu\varepsilon}\Delta\boldsymbol{\varepsilon} + \mathbf{C}_{\mu\eta}\Delta\boldsymbol{\eta}\right) - \Delta D\left(\mathbf{C}_{\mu\varepsilon}\boldsymbol{\varepsilon}^{i-1} + \mathbf{C}_{\mu\eta}\boldsymbol{\eta}^{i-1}\right). \end{aligned} \tag{6}$$

Incremental change of the damage variable in Eq. (6) is approximated by

$$\Delta D = \left(\frac{\mathrm{d}D}{\mathrm{d}\boldsymbol{\varepsilon}} \right)^{i-1} \Delta\boldsymbol{\varepsilon}, \tag{7}$$

where the damage variable derivative with respect to the strain tensor can be found in the analytical manner. Employing the relations given in [11], strain and second-order strain increments can be expressed in the terms of the nodal displacement increment vector $\Delta\mathbf{v}$ by the relations

$$\begin{aligned} \Delta\boldsymbol{\varepsilon} &= \mathbf{B}_{\varepsilon}\Delta\mathbf{v}, \\ \Delta\boldsymbol{\eta} &= \mathbf{B}_{\eta}\Delta\mathbf{v}. \end{aligned} \tag{8}$$

Substitution of the Eqs. (6)-(8) in the Eq. (4) gives after some straightforward manipulation the following non-linear finite element equation

$$\left(\mathbf{K}_{\varepsilon\varepsilon} + \mathbf{K}_{\varepsilon\eta} + \mathbf{K}_{\eta\varepsilon} + \mathbf{K}_{\eta\eta} \right) \Delta\mathbf{v} = \mathbf{F}_{\mathrm{e}} - \mathbf{F}_{\mathrm{i}}, \tag{9}$$

with particular element stiffness matrices defined as

$$\begin{aligned} \mathbf{K}_{\varepsilon\varepsilon} &= \int_A \mathbf{B}_{\varepsilon}^T \left[\left(1 - D^{i-1}\right)\mathbf{C}_{\sigma\varepsilon} - \mathbf{C}_{\sigma\varepsilon}\boldsymbol{\varepsilon}^{i-1} \left(\frac{\mathrm{d}D}{\mathrm{d}\boldsymbol{\varepsilon}} \right)^{i-1} - \mathbf{C}_{\sigma\eta}\boldsymbol{\eta}^{i-1} \left(\frac{\mathrm{d}D}{\mathrm{d}\boldsymbol{\varepsilon}} \right)^{i-1} \right] \mathbf{B}_{\varepsilon} \mathrm{d}A, \\ \mathbf{K}_{\varepsilon\eta} &= \int_A \mathbf{B}_{\varepsilon}^T \left(1 - D^{i-1}\right) \mathbf{C}_{\sigma\eta} \mathbf{B}_{\eta} \,\mathrm{d}A, \\ \mathbf{K}_{\eta\varepsilon} &= \int_A \mathbf{B}_{\eta}^T \left[\left(1 - D^{i-1}\right)\mathbf{C}_{\mu\varepsilon} - \mathbf{C}_{\mu\varepsilon}\boldsymbol{\varepsilon}^{i-1} \left(\frac{\mathrm{d}D}{\mathrm{d}\boldsymbol{\varepsilon}} \right)^{i-1} - \mathbf{C}_{\mu\eta}\boldsymbol{\eta}^{i-1} \left(\frac{\mathrm{d}D}{\mathrm{d}\boldsymbol{\varepsilon}} \right)^{i-1} \right] \mathbf{B}_{\varepsilon} \mathrm{d}A, \\ \mathbf{K}_{\eta\eta} &= \int_A \mathbf{B}_{\eta}^T \left(1 - D^{i-1}\right) \mathbf{C}_{\mu\eta} \mathbf{B}_{\eta} \,\mathrm{d}A. \end{aligned} \tag{10}$$

External and internal force vectors, $\mathbf{F}_{\mathrm{e}}$ and $\mathbf{F}_{\mathrm{i}}$ respectively, are obtained as

$$\begin{aligned} \mathbf{F}_{\mathrm{e}} &= \int_s \left(\mathbf{N}^T \mathbf{t} + \mathrm{grad}\,\mathbf{N}^T \mathbf{T} \right) \mathrm{d}s, \\ \mathbf{F}_{\mathrm{i}} &= \int_A \left(\mathbf{B}_{\varepsilon}^T \boldsymbol{\sigma}^{i-1} + \mathbf{B}_{\eta}^T \boldsymbol{\mu}^{i-1} \right) \mathrm{d}A. \end{aligned} \tag{11}$$

Presented damage formulation has been implemented into the two-dimensional C^1 continuity triangular finite element [11] using the FE program ABAQUS and its user element subroutine UEL [13].

3 Numerical example

In the following chapter the algorithm presented above is verified on a benchmark example tested also in [9], where only the homogeneous material was taken into account. Here, the heterogeneous material was also included in the simulations.

3.1 Plate with an imperfect zone – model problem description

The problem considered consists of the rectangular domain and boundary conditions shown in Fig. 2. At the right edge displacement of 0.0325 mm is imposed. In order to trigger localization, Young's modulus in the middle hatched area of the plate is reduced by 10%, and for the rest of the plate is taken as $E = 20000$ N/mm^2. Poisson's ratio is equal to $\nu = 0.25$, while the damage evolution parameters are set to $k_0 = 0.0001$ and $k_u = 0.0125$.

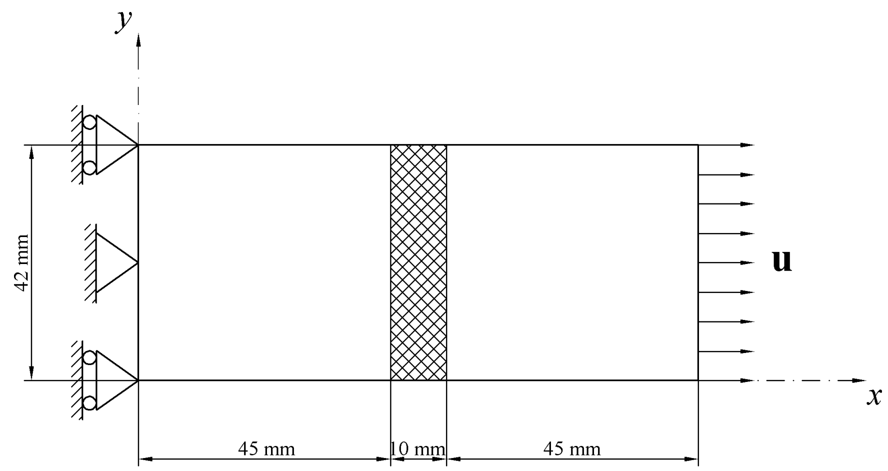

Figure2: Geometry and boundary conditions of the plate model

3.2 Homogeneous material

As it has been stated above, material tangent stiffness matrices $\mathbf{C}_{\sigma\eta}$ and $\mathbf{C}_{\mu\varepsilon}$ are for the homogeneous and isotropic material both equal to zero. Thus, incremental constitutive relations represented by Eq. (6) now read

$$\begin{aligned} \Delta\boldsymbol{\sigma} &= (1 - D^{i-1})\mathbf{C}_{\sigma\varepsilon}\Delta\boldsymbol{\varepsilon} - \Delta D\mathbf{C}_{\sigma\varepsilon}\boldsymbol{\varepsilon}^{i-1}, \\ \Delta\boldsymbol{\mu} &= (1 - D^{i-1})\mathbf{C}_{\mu\eta}\Delta\boldsymbol{\eta} - \Delta D\mathbf{C}_{\mu\eta}\boldsymbol{\eta}^{i-1}. \end{aligned} \tag{12}$$

Remaining two tangent stiffness matrices can be found either analytically or numerically, using the homogenization procedure. Analytical expressions for $\mathbf{C}_{\sigma\varepsilon}$ and $\mathbf{C}_{\mu\eta}$ can be found in [10], and here only their short form is given as

$$\mathbf{C}_{\sigma\varepsilon} = \mathbf{C}_{\sigma\varepsilon}\left(E,\nu\right),$$
$$\mathbf{C}_{\mu\eta} = \mathbf{C}_{\mu\eta}\left(E,\nu,L\right), \tag{13}$$

where L denotes the size of the microstructural representative volume element. It is shown in [14] that, in the second-order computational homogenization scheme, RVE size L can be linked to the internal length scale of the resulting macroscopic homogenized higher-order continuum l, as follows

$$l^2 = \frac{L^2}{12}. \tag{14}$$

In the homogenization procedure three different sizes of the RVE were used in order to examine the effects of the internal length scale parameter on the results. For this purpose, RVE side lengths of L = 5.2 mm (l = 1.5 mm), 6.9 mm (l = 2.0 mm) and 10.4 mm (l = 3.0 mm) were tested, with the RVE discretization shown in Fig. 3.

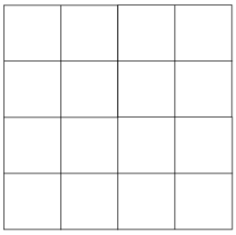

Figure3: Homogeneous RVE discretization, 16 elements

3.2.1 Mesh independence

In order to examine convergence and mesh objectivity of the presented algorithm, results from three different discretization layouts were compared. The coarsest mesh consists of 5x10 nodes (72 elements) and it is shown in Fig. 4. The other two discretizations are of the same form and have the following nodal layouts: 9x21 nodes (320 elements) and 17x41 nodes (1280 elements).

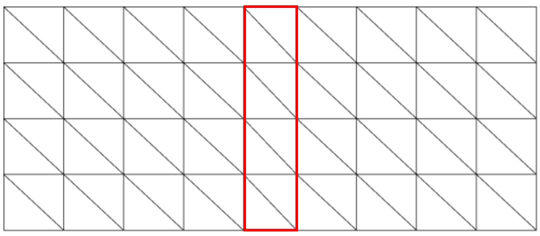

Figure4: The coarsest mesh consisting of 5x10 nodes (72 elements)

Fig. 5 shows the comparison of the computed damage variable profiles for displacement $u = 0.0325$ mm along the horizontal central axis for three different discretization cases. Results were obtained using the homogenized material tangent stiffness matrices and the internal length scale parameter $l = 1.5$ mm. It can be noted that the results are almost identical. Deviations in the center of the plate and in the transition zones where the damage variable starts to grow exist only due to linear approximation lines connecting the node values.

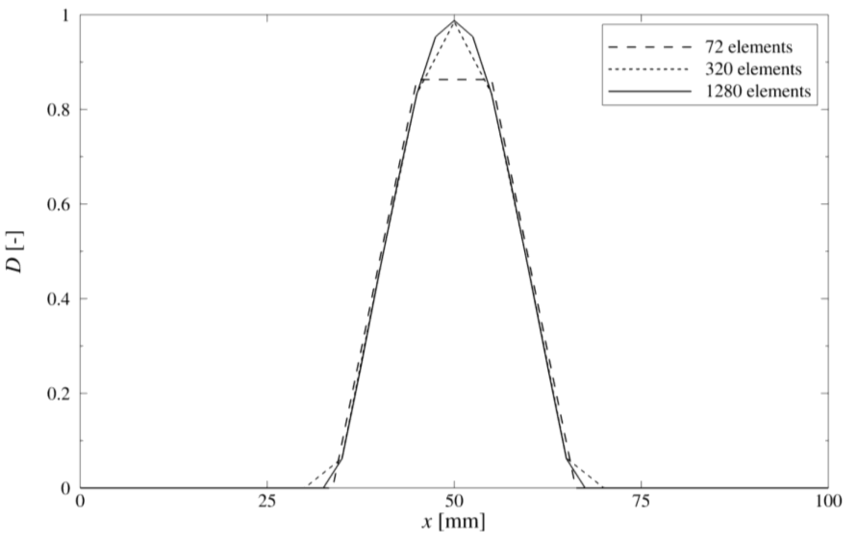

Figure5: Comparison of damage profile for homogeneous material along the horizontal central axis for three different discretizations at $u = 0.0325$ mm

3.2.2 Effect of the internal length scale parameter

Using the homogenized material stiffness matrices three different RVE side lengths were tested in order to observe the effect of the internal length scale parameter on a damage profile, as shown in Fig. 6. It is obvious that the change of the internal length scale parameter affects the size of the localization zone, in such a way that with the increase of the internal length scale parameter localization zone becomes wider and peak value of the damage variable decreases. This is in correlation to the definition of the internal length scale parameter, which states that the mentioned parameter depicts intensity of the microstructural interaction.

3.2.3 Evolution of damage variable and equivalent elastic strain

Fig. 7 and Fig. 8 illustrate evolution of the damage process over eight displacement increments ranging from $u = 0$ to $u = 0.0325$ mm. In Fig. 7 this evolution is described by plotting the damage variable, and in Fig. 8 evolution of the corresponding equivalent elastic strain needed for the damage variable calculation is given. As it can be seen, strain localizes in the zone of the unchanging width immediately at the onset of the softening, and in the subsequent stages tends to the higher values only in the middle of the plate. This behavior shows the tendency of the strain to localize mainly into a line in the middle of the plate where cracking will happen eventually, as it can be observed in the behavior of the real materials. Also, it can be noted that the damage variable shows a rapid increase at the beginning of the softening, while subsequently this growth is reduced to a minimum. More detailed behavior of the linear and other softening laws can be seen in [2].

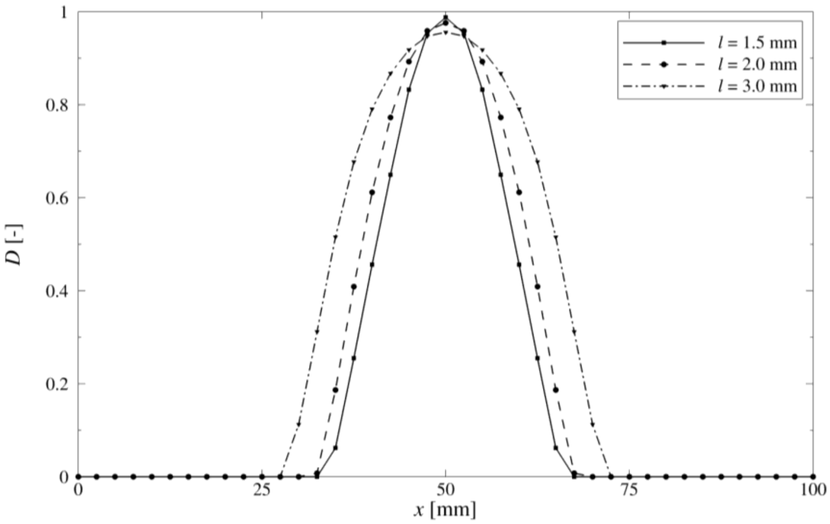

Figure6: Comparison of damage profile for homogeneous material along the horizontal central axis for three different values of internal length scale parameter l at u = 0.0325 mm

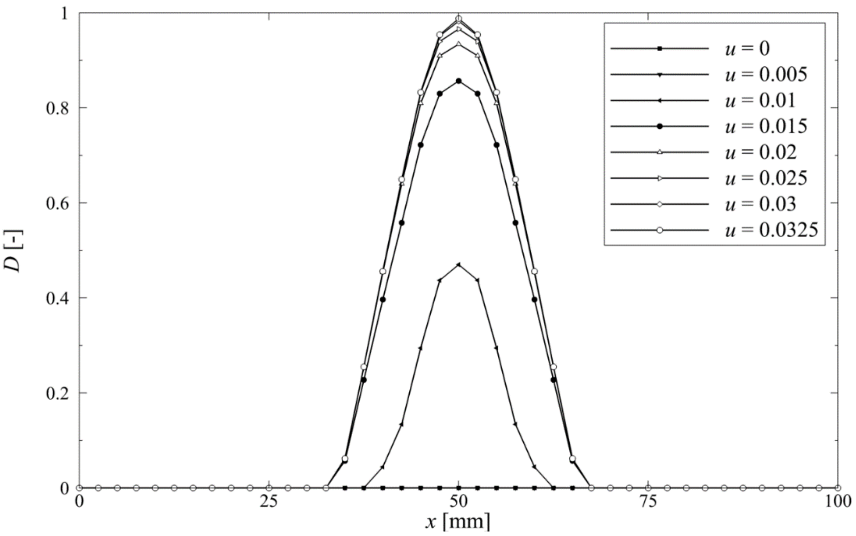

Figure7: Evolution of damage variable D along horizontal central axis for homogeneous material and internal length scale parameter l = 1.5 mm; displacement u is in mm

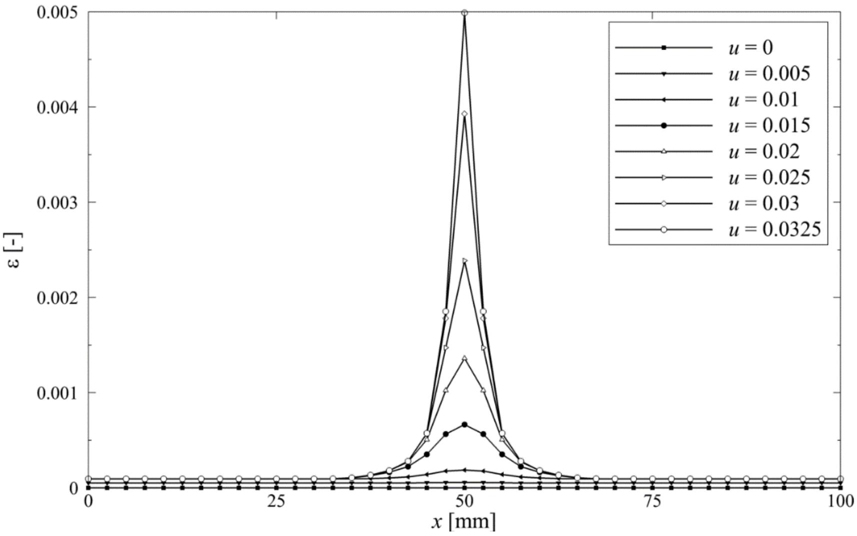

Figure8: Evolution of equivalent elastic strain ε along horizontal central axis for homogeneous material and internal length scale parameter l = 1.5 mm; displacement u is in mm

3.2.4 Contour plots

Distribution of the damage variable D given in Fig. 9 and distribution of the equivalent elastic strain ε shown in Fig. 10 refer to a highly localized deformation state at u = 0.0325 mm and the internal length scale parameter l = 1.5 mm. Both the damage variable and the equivalent elastic strain widen near the top and bottom edge where the contribution of the lateral contraction is more pronounced.

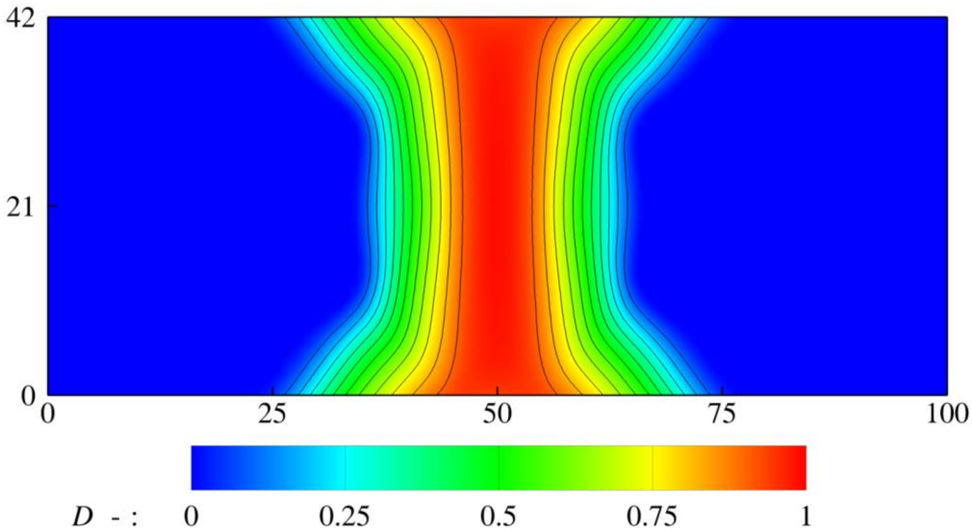

Figure9: Distribution of damage variable D for homogeneous material and internal length scale parameter l = 1.5 mm *at* u = 0.0325 mm

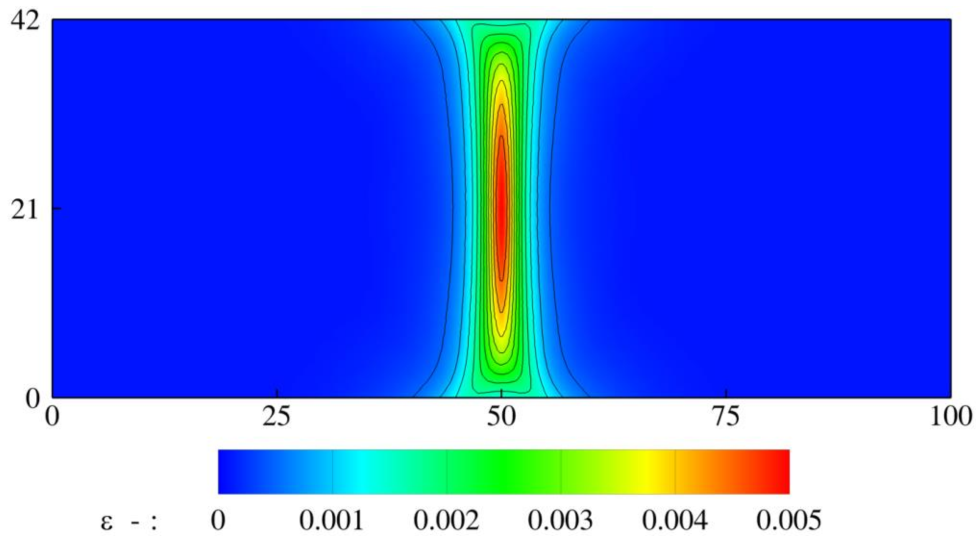

Figure10: Distribution of equivalent elastic strain ε for homogeneous material and internal length scale parameter l = 1.5 mm *at* u = 0.0325 mm

3.3 Heterogeneous material

In the case of a heterogeneous material, full form of the incremental constitutive relations represented by Eq. (6) has to be solved. For the computation of the material tangent stiffness matrices an academic RVE example with 13% porosity was used in the homogenization procedure, as shown in Fig. 11.

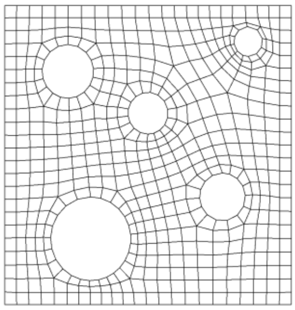

Figure11: Heterogeneous RVE consisting of 508 elements

RVE has the side length L = 5.2 mm, i.e. it represents the microstructure of the internal length scale parameter l = 1.5 mm. In Fig. 12 comparison of the damage profiles obtained by both heterogeneous and homogeneous material of the same internal length scale parameter at the overall stretch u = 0.0325 mm is made. Obviously, noticeable differences can be observed. It can also be seen that heterogeneous damage profile is not symmetric, which could be attributed to the lack of statistical representativeness of the RVE. However, influence of the RVE size and porosity on the damage response will be investigated in the further research.

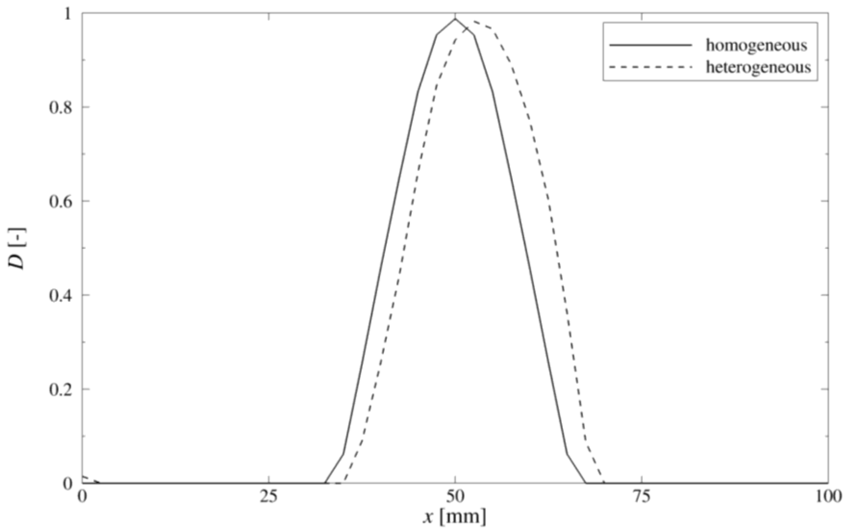

Figure12: Comparison of damage profile along the horizontal central axis for the homogeneous and heterogeneous material, for internal length scale l = 1.5 mm and at u = 0.0325 mm

4 Conclusion

Damage model in the context of the full strain gradient continuum has been presented. Model has been based on the isotropic damage law so that all four material tangent stiffness matrices appearing in the constitutive relations are pre-multiplied by the same term that describes damage process. This highly non-linear softening behavior was implemented into the triangular C^1 element using the FE software ABAQUS and the provided UEL subroutine. Applicability and efficiency of the presented algorithm were demonstrated on a typical benchmark example of a stretched plate weakened in the middle. Homogeneous and heterogeneous materials were analyzed by employing the second-order homogenization procedure to obtain the required material matrices. From comparison of the results obtained by three different finite element discretizations it was concluded that model is mesh independent. Effect of the internal length scale parameter was observed, showing that the model derived is capable of capturing intensity of the microstructural interactions. Evolution of the softening process was studied and overall behavior of the softening process was given by plotting damage variable and equivalent elastic strain field distributions. Comparison of homogeneous and heterogeneous material showed different damage responses. Further research on heterogeneous materials is yet to come.

Acknowledgments

The investigation described in this paper is the part of the project “Multiscale Numerical Modeling of Material Deformation Responses from Macro- to Nanolevel” – MnumMacroNano, supported by the Croatian Science Foundation under contract HRZZ IP-11-2013-2516.

References

[1] Lemaitre, J. *A Course on Damage Mechanics*, 2^{nd} edition. Springer, Berlin, 1996

[2] Peerlings, R.H.J. *Enhanced damage modeling for fracture and fatigue*. Ph.D. Thesis, Eindhoven University of Technology, The Netherlands, 1999.

[3] Bažant, Z.P., Belytschko, T. and Chang, T.P. Continuum theory for strain-softening. *J.Eng. Mech*., 110, 1666–1692, 1984.

[4] Peerlings, R.H.J., de Borst, R., Brekelmans,W., Geers, M.G.D. Gradient-enhanced damage modeling of concrete fracture. *Mechanics of Cohesive-Frictional Materials*, 3, 323–342, 1998.

[5] de Borst, R. and Mühlhaus, H.B. Gradient-dependent plasticity: formulation and algorithmic aspects. *Int. J. Num. Meth. Eng.*, 35, 521–539, 1992.

[6] Sluys, L.J.; de Borst, R.; Mühlhaus, H.B. Wave propagation, localization and dispersion in a gradient-dependent medium. *International Journal of Solidsand Structures*, vol. 30, pp. 1153-1171, 1993.

[7] Askes H., Sluys L.J. Explicit and implicit gradient series in damage mechanics. *European Journal of Mechanics a-Solids*. 21(3):379-90, 2002.

[8] Chang, C.S.; Askes, H.; Sluys, L.J. (2002), Higher-order strain/higher-order stress gradient models derived from a discrete microstructure, with application to fracture. *Engineering Fracture Mechianics*, vol. 69, pp. 1907-1924, 2002.

[9] Yang, Y., A. Misra, A. Higher-Order Stress-Strain Theory for Damage Modeling Implemented in an Element-free Galerkin Formulation. *CMES: Computer Modeling in Engineering and Sciences*, 64, 1-36, 2011.

[10] Kaczmarczyk L, Pearce C.J., Bićanić N. Scale transition and enforcement of RVE boundary conditions in second-order computational homogenization. *Int J Numer Methods Eng*, 74:506–522, 2008.

[11] Lesičar T., Tonković Z., Sorić J. A second-order two-scale homogenization procedure using C-1 macrolevel discretization. *Computational Mechanics*, 2014;54(2):425-41, 2014.

[12] Akarapu S., Zbib H.M. Numerical analysis of plane cracks in strain-gradient elastic materials. *International Journal of Fracture*, 141(3-4):403-30, 2006.

[13] Abaqus/Standard 6.13.1. Dassault Systemes, Simulia, 2014.

[14] Kouznetsova V.G., Geers M.G.D., Brekelmans W.A.M. Multiscale second-order computational homogenization of multi-phase materials: a nested finite element solution strategy. *Comput Methods Appl Mech Eng*, 193:5525–5550, 2004.